J|A|C|S
ARTICLES

Published on Web 12/09/2010

Evidence for a Near-Resonant Charge Transfer Mechanism for Double-Stranded Peptide Nucleic Acid

Ravindra Venkatramani,[II,†] Kathryn L. Davis,[II,‡] Emil Wierzbinski,[‡] Silvia Bezer,[§] Alexander Balaeff,[†] Shahar Keinan,[†] Amit Paul,[‡] Laura Kocsis,[§] David N. Beratan,*[,#] Catalina Achim,*[,§] and David H. Waldeck*[,‡]

Departments of Chemistry, Biochemistry, and Physics, Duke University, Durham, North Carolina 27708; Department of Chemistry, University of Pittsburgh, Pittsburgh, Pennsylvania 15260; and Department of Chemistry, Carnegie Mellon University, Pittsburgh, Pennsylvania 15213

Received August 23, 2010; E-mail: david.beratan@duke.edu; achim@cmu.edu; dave@pitt.edu

Abstract: We present evidence for a near-resonant mechanism of charge transfer in short peptide nucleic acid (PNA) duplexes obtained through electrochemical, STM break junction (STM-BJ), and computational studies. A seven base pair (7-bp) PNA duplex with the sequence $(TA)_3$-(XY)-$(TA)_3$ was studied, in which XY is a complementary nucleobase pair. The experiments showed that the heterogeneous charge transfer rate constant (k^0) and the single-molecule conductance (σ) correlate with the oxidation potential of the purine base in the XY base pair. The electrochemical measurements showed that the enhancement of k^0 is independent, within experimental error, of which of the two PNA strands contains the purine base of the XY base pair. 7-bp PNA duplexes with one or two GC base pairs had similar measured k^0 and conductance values. While a simple superexchange model, previously used to rationalize charge transfer in single stranded PNA (Paul et al. *J. Am. Chem. Soc.* **2009**, *131*, 6498−6507), describes some of the experimental observations, the model does not explain the absence of an enhancement in the experimental k^0 and σ upon increasing the G content in the duplexes from one to two. Moreover, the superexchange model is not consistent with other studies (Paul et al. *J. Phys. Chem. B* **2010**, *114,* 14140), that showed a hopping charge transport mechanism is likely important for PNA duplexes longer than seven base pairs. A quantitative computational analysis shows that a near-resonant charge transfer regime, wherein a mix of superexchange and hopping mechanisms are expected to coexist, can rationalize all of the experimental results.

Introduction

The realization of artificial supramolecular machines that perform multielectron chemistry requires the development of new methods and concepts for creating and understanding how to organize electroactive units so that they function cooperatively. A great deal of work over the last two decades has focused on developing an understanding of the fundamental processes underlying charge transfer in DNA.[1] Since the charge transport properties of DNA are sensitive to the nucleobase sequence, nucleic acids could be used as tunable components.[2−4] Sequence variability, intrinsic molecular recognition, and supramolecular self-assembly capabilities[5−9] make nucleic acids prime candidates for realizing such machines.

We have been exploring the charge transfer properties of PNA, a synthetic analogue of DNA.[10−12] PNA has the advantages of charge neutrality (allowing the formation of high surface coverage self-assembled monolayers, or SAMs), amenability to chemical modification (e.g., attachment of metal complexes), and resistance to enzymatic decomposition. We have studied the effects of nucleobase energetics on charge transfer through single-stranded (ss) PNAs of the form Cys-T_3-X-T_3-Fc, (Cys = cysteine that binds to a gold electrode, Fc = ferrocene that serves as an electrochemical redox reporter, and X = C, T, A,

[†] Department of Chemistry, Duke University.
[‡] Department of Chemistry, University of Pittsburgh.
[§] Department of Chemistry, Carnegie Mellon University.
[#] Departments of Chemistry, Biochemistry and Physics, Duke University.
[II] These two authors contributed equally to the work.

(1) Long-Range Charge Transfer in DNA I and II. In *Topics in Current Chemistry*; Schuster, G. B., Ed.; Springer: Berlin/Heidelberg, 2004; Vols. 236 and 237.
(2) Kawai, K.; Kodera, H.; Majima, T. *J. Am. Chem. Soc.* **2009**, *132*, 627.
(3) Kawai, K.; Kodera, H.; Osakada, Y.; Majima, T. *Nat. Chem.* **2009**, *1*, 156.
(4) Taniguchi, M.; Kawai, T. *Phys. E* **2006**, *33*, 1.
(5) Hazarika, P.; Ceyhan, B.; Niemeyer, C. M. *Angew. Chem., Int. Ed.* **2004**, *43*, 6469.
(6) LaBean, T. H.; Yan, H.; Kopatsch, J.; Liu, F.; Winfree, E.; Reif, J. H.; Seeman, N. C. *J. Am. Chem. Soc.* **2000**, *122*, 1848.
(7) Seeman, N. C. *J. Theor. Biol.* **1982**, *99*, 237.
(8) Seeman, N. C. *Annu. Rev. Biophys. Biomol. Struct.* **1998**, *27*, 225.
(9) Seeman, N. C. *Nature* **2003**, *421*, 427.
(10) Paul, A.; Watson, R. M.; Wierzbinski, E.; Davis, K. L.; Sha, A.; Achim, C.; Waldeck, D. H. *J. Phys. Chem. B* **2010**, *114*, 14140.
(11) Paul, A.; Bezer, S.; Venkatramani, R.; Kocsis, L.; Wierzbinski, E.; Balaeff, A.; Keinan, S.; Beratan, D. N.; Achim, C.; Waldeck, D. H. *J. Am. Chem. Soc.* **2009**, *131*, 6498.
(12) Paul, A.; Watson, R. M.; Lund, P.; Xing, Y.; Burke, K.; He, Y.; Borguet, E.; Achim, C.; Waldeck, D. H. *J. Phys. Chem. C* **2008**, *112*, 7233.

 10.1021/ja107622m

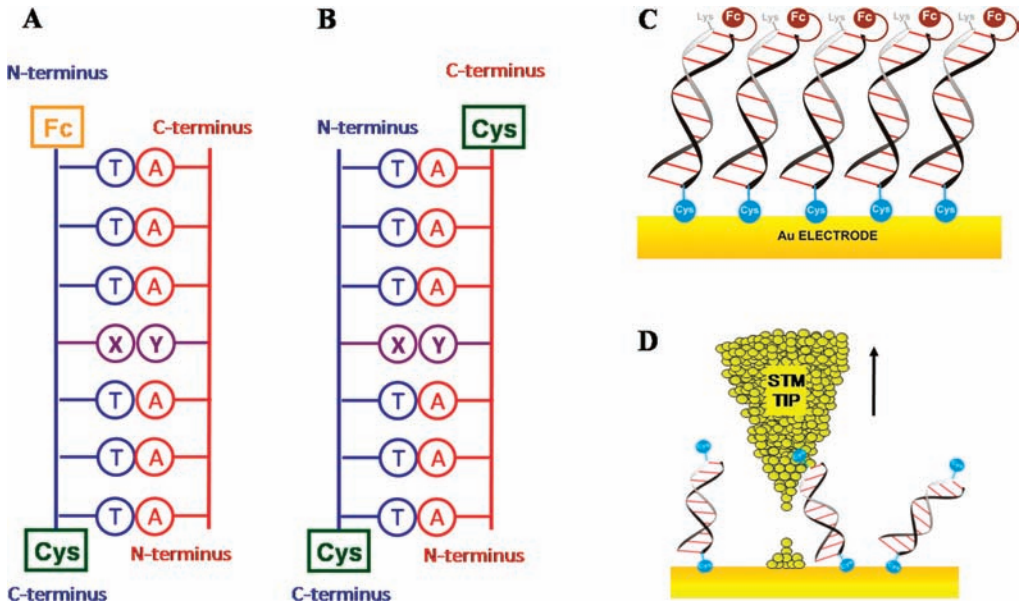

Figure 1. Schematic views of the PNA systems and experimental techniques. XY denotes a central AT, TA, CG, or GC base pair. The C- and N-termini are marked for each PNA strand. A: Ferrocene (Fc)-terminated PNAs used in cyclic voltammetry experiments. B: Cysteine (Cys)-terminated PNAs used in STM break-junction experiments. Cys and Fc moieties are attached to the C- and N-termini of the PNA, respectively. C: Fc-terminated PNA SAMs on gold electrodes used in cyclic voltammetry studies. D: STM break junction measurement of single-molecule PNA conductance.

or G). The results showed that charge transfer through ss PNA SAMs takes place through the bases on the same strand (rather than cross-strand or through the backbone) via hole-mediated superexchange.[11] The measured k^0 values in ss PNA depend strongly on the oxidation potential of the central nucleobase X and correlate well with theoretical conductance values. These experimental observations were found to be consistent with an ensemble-averaged superexchange model. Distance dependence studies of k^0 in ss PNA of 3 to 7 nucleobases found a characteristic tunneling decay length of 0.86/Å for T-strands and 0.76/Å for A-strands.[10] k^0 for longer ss PNA and ds PNA strands had a softer distance dependence.[10] This behavior is reminiscent of the transition from superexchange to hopping transport that was reported for DNA duplexes.[13−15]

Here we report on charge transfer through SAMs composed of ds PNA Cys-$(TA)_3$-(XY)-$(TA)_3$-Fc (Figure 1A and C), where XY is a complementary base pair (AT, CG, TA, and GC). We use cyclic voltammetry (Figure 1A,C), STM break junction (STM-BJ) experiments (Figure 1B,D),[16] and theoretical studies to understand charge transfer in these ds PNAs. The results of the experimental electrochemical and STM-BJ studies lead to three major observations about charge transfer: (1) the electrochemical rate constant k^0 and the molecular conductance σ correlate with the oxidation potential of the purine in the XY base pair, (2) k^0 is insensitive to which duplex strand binds the purine of the XY base pair; and (3) increasing the G content of the duplex from one to two does not enhance k^0 and σ. Theoretical calculations of σ for a molecular dynamics ensemble of duplex PNA structures were carried out in the superexchange and near-resonant charge transport regimes using the nonequilibrium Green's function method. The theoretical analysis showed that the charge transfer mechanism is near-resonant and that bridge dephasing is necessary to rationalize the experimental observations. This near-resonant mechanism in ds PNA contrasts with the hole-mediated superexchange transport found to operate in ss PNA.[11]

Table 1. Electrochemical Results for ds-PNA SAMs along with Oxidation Potentials for Isolated X and Y Nucleobases in Figure 1

PNA duplex[a]	k^0(s^{-1})	surface coverage (pmol/cm^2)	E_{Ox}(X)[b] (V)	E_{Ox}(Y)[b] (V)
Cys-TTT-**C**-TTT-Fc	0.67 ± 0.16	70 ± 20	1.90	1.25
Cys-TTT-**T**-TTT-Fc	0.25 ± 0.05	110 ± 40	1.87	1.72
Cys-TTT-**A**-TTT-Fc	0.32 ± 0.06	70 ± 50	1.72	1.87
Cys-TTT-**G**-TTT-Fc	0.57 ± 0.14	120 ± 50	1.25	1.90
Cys-AAG-**T**-TGT-Fc	0.58 ± 0.20	100 ± 30	N/A	N/A

[a] Shown is the PNA strand of the duplex that contains the Fc redox reporter. The nucleobase **X** is shown in bold; **Y** is the complementary nucleobase. [b] Taken from ref 19. All voltages are reported with respect to the Ag/AgCl reference electrode.

Results

Charge transfer through the PNA bridge was monitored using an N-terminal Fc redox reporter. The surface coverage of the PNA duplexes was evaluated by ellipsometry and by integrating the charge under the voltammograms (see Table 1 for the coverages and the Supporting Information for a detailed description). Figure 2 shows cyclic voltammograms at scan rates of 10, 20, and 30 mV/s as well as the dependence of the peak position on scan rate, or trumpet plots, for electrodes coated with self-assembled monolayers (SAMs) of ds PNA of the sequence Cys-T_3-T-T_3-Fc:Lys-A_3-A-A_3, Cys-T_3-G-T_3-Fc:Lys-A_3-C-A_3, and Cys-A_2-G-T_2-G-T-Fc:Lys-A-C-A_2-C-T_2. The trumpet plots were fitted by a curve derived from Marcus theory in order to determine k^0, the standard heterogeneous rate constant.[17,18] The charge transfer rate constants determined for each

(13) Lewis, F. D.; Zhu, H. H.; Daublain, P.; Fiebig, T.; Raytchev, M.; Wang, Q.; Shafirovich, V. *J. Am. Chem. Soc.* **2006**, *128*, 791.
(14) Giese, B.; Amaudrut, J.; Kohler, A.-K.; Spormann, M.; Wessely, S. *Nature* **2001**, *412*, 318.
(15) Berlin, Y. A.; Kurnikov, I. V.; Beratan, D.; Ratner, M. A.; Burin, A. L. In *Long-Range Charge Transfer in DNA II*; Schuster, G. B., Ed.; Springer: Berlin/Heidelberg, 2004; Vol. 237, p 1.
(16) Xu, B.; Tao, N. J. *Science* **2003**, *301*, 1221.
(17) Napper, A. M.; Liu, H.; Waldeck, D. H. *J. Phys. Chem. B* **2001**, *105*, 7699.

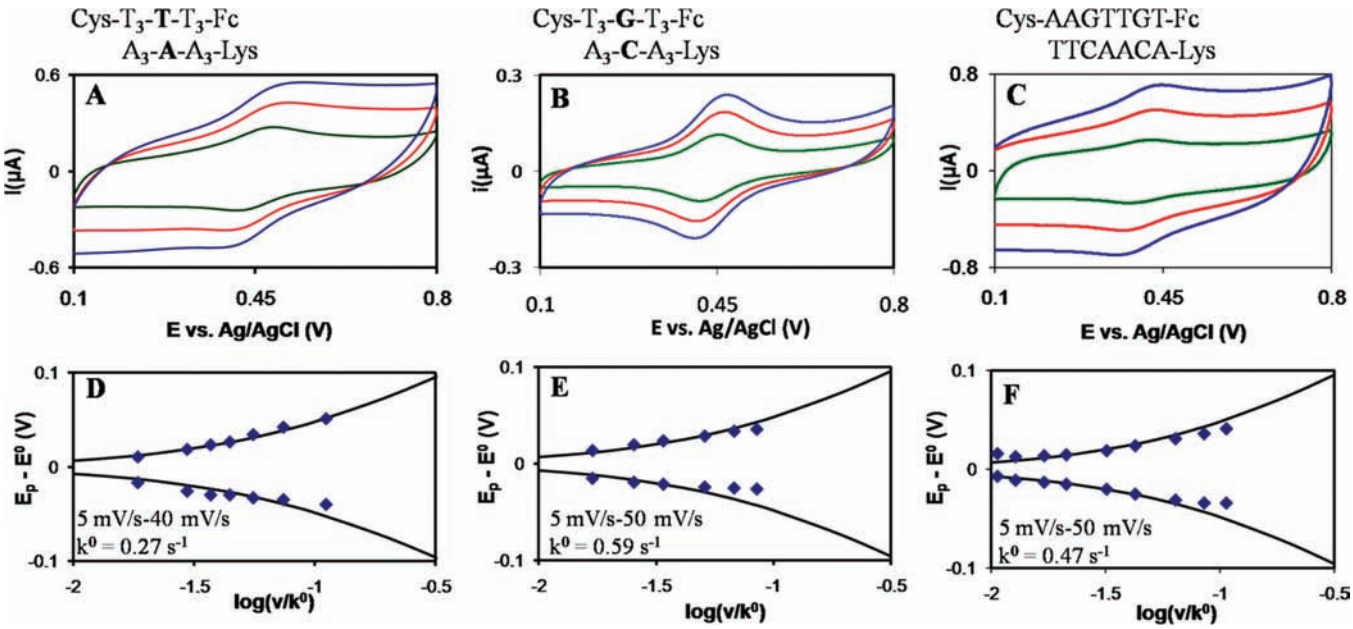

Figure 2. Voltammograms and Marcus theory fitting curves for SAMs of Cys-T_3-T-T_3-Fc:Lys-A_3-A-A_3 (A and D), Cys-T_3-G-T_3-Fc:Lys-A_3-C-A_3 (B and E), and Cys-AAGTTGT-Fc:Lys-ACAACTT (C and F). The voltammograms were taken in 1 M $NaClO_4$ solution at scan rates of 10 (green), 20 (red), and 30(blue) mV/s.

of the ds PNA SAMs are summarized in Table 1. The typical surface coverage was the same for all ds PNA SAMs, as confirmed by *t* tests at 95% confidence, and is near 100 pmol/cm^2.

The data in Figure 2 and Table 1 reveal three major observations. First, k^0 for GC-containing PNAs are larger than for AT-only PNAs; this finding is consistent with data reported for DNA.[20,21] Second, the k^0 rate is not sensitive to the relative strand location of the purine base of the XY pair; that is, Rate[Cys-$(TA)_3$-(GC)-$(TA)_3$-Fc] ≈ Rate[Cys-$(TA)_3$-(CG)-$(TA)_3$-Fc] and Rate[Cys-$(TA)_3$-(AT)-$(TA)_3$-Fc] ≈ Rate[Cys-$(TA)_3$-(TA)-$(TA)_3$-Fc]. This observation is unexpected in light of observations previously made for DNA. For DNA, the interstrand location of the purines led to an attenuation of charge transfer.[22−24] Lastly, k^0 for the 7-bp duplex Cys-AAGTTGT-Fc:Lys-ACAACTT, which contains two GC pairs, is similar to that for Cys-T_3-G-T_3-Fc:Lys-A_3-C-A_3, which contains only one GC pair.

Measurements of Single Molecule Conductance. The conductance of PNA molecules was measured using the STM-controlled break-junction method.[16] In this experiment, loosely packed PNA molecules are occasionally trapped on the substrate surface between the substrate and an STM tip by periodic modulation of the tip−substrate separation (Figure 1D). During this process, the tunneling current is monitored as a function of the tip−substrate distance at a constant bias voltage. The conductance is determined by statistical analysis of current-distance characteristics, such as those shown in Figure 3A. Conductance distributions that were constructed from multiple measurements of current-distance characteristics for the Cys-A_3-A-A_3:Cys-T_3-T-T_3, Cys-A_3-G-A_3:Cys-T_3-C-T_3, and Cys-AAGTTGT:Cys-ACAACTT duplexes are shown in Figure 3B−D, respectively. The figures show a fit of the distributions to a sum of Gaussians, which was used to make peak assignments (see Table 2). The distributions observed for Cys-A_3-A-A_3:Cys-T_3-T-T_3 and Cys-A_3-G-A_3:Cys-T_3-C-T_3 (Figure 3B,C) have similar median conductance values and display two characteristic regions: a narrow one (at 0.0003−0.0030 G_0) and a broad one at (0.0030−0.0150 G_0). It is unlikely that the clustering in these two regions is caused by the presence of several molecules in the junction during measurement because, in such a case, one would observe integral multiples of the fundamental conductance value measured for a single molecule at the junction.[16,25] A likely explanation is that the two regions correspond to molecules with different conformations or contact geometries, with the higher molecular conductance range being attributed to a geometry and/or contact configuration that is more favorable for charge transfer.[26−30]

The observed mean, median, and fundamental conductance values for the three PNA duplexes (Cys-A_3-A-A_3:Cys-T_3-T-T_3, Cys-A_3-G-A_3:Cys-T_3-C-T_3, and Cys-AAGTTGT:Cys-ACAACTT) are given in Table 2. The mean conductance value increases slightly with the guanine content of the duplex. The median conductance of the sequence containing a single GC is larger by about 35% than for the all-AT sequence (5.5×10^{-3} G_0 vs

(18) Weber, K.; Creager, S. E. *Anal. Chem.* **1994**, *66*, 3164.
(19) Seidel, C. A. M.; Schulz, A.; Sauer, M. H. M. *J. Phys. Chem.* **1996**, *100*, 5541.
(20) Lewis, F. D.; Daublain, P.; Cohen, B.; Vura-Weis, J.; Wasielewski, M. R. *Angew. Chem., Int. Ed.* **2008**, *47*, 3798.
(21) Nakatani, K.; Dohno, C.; Saito, I. *J. Am. Chem. Soc.* **2000**, *122*, 5893.
(22) Kelley, S. O.; Barton, J. K. *Science* **1999**, *283*, 375.
(23) Lewis, F. D.; Zuo, X.; Liu, J.; Hayes, R. T.; Wasielewski, M. R. *J. Am. Chem. Soc.* **2002**, *124*, 4568.
(24) Long, Y.-T.; Li, C.-Z.; Sutherland, T. C.; Chahma, M. h.; Lee, J. S.; Kraatz, H.-B. *J. Am. Chem. Soc.* **2003**, *125*, 8724.
(25) Cui, X. D.; Primak, A.; Zarate, X.; Tomfohr, J.; Sankey, O. F.; Moore, A. L.; Moore, T. A.; Gust, D.; Harris, G.; Lindsay, S. M. *Science* **2001**, *294*, 571.
(26) Li, C.; Pobelov, I.; Wandlowski, T.; Bagrets, A.; Arnold, A.; Evers, F. *J. Am. Chem. Soc.* **2007**, *130*, 318.
(27) Li, X.; He, J.; Hihath, J.; Xu, B.; Lindsay, S. M.; Tao, N. *J. Am. Chem. Soc.* **2006**, *128*, 2135.
(28) Martin, S.; Giustiniano, F.; Haiss, W.; Higgins, S. J.; Whitby, R. J.; Nichols, R. J. *J. Phys. Chem. C* **2009**, *113*, 18884.
(29) Omori, Y.; Tobita, J.; Kato, Y.; Uichi, Akiba; Fujihira, M. *Jpn. J. Appl. Phys.* **2007**, *46*, 7829.
(30) Wierzbinski, E.; Slowinski, K. *Langmuir* **2006**, *22*, 5205.

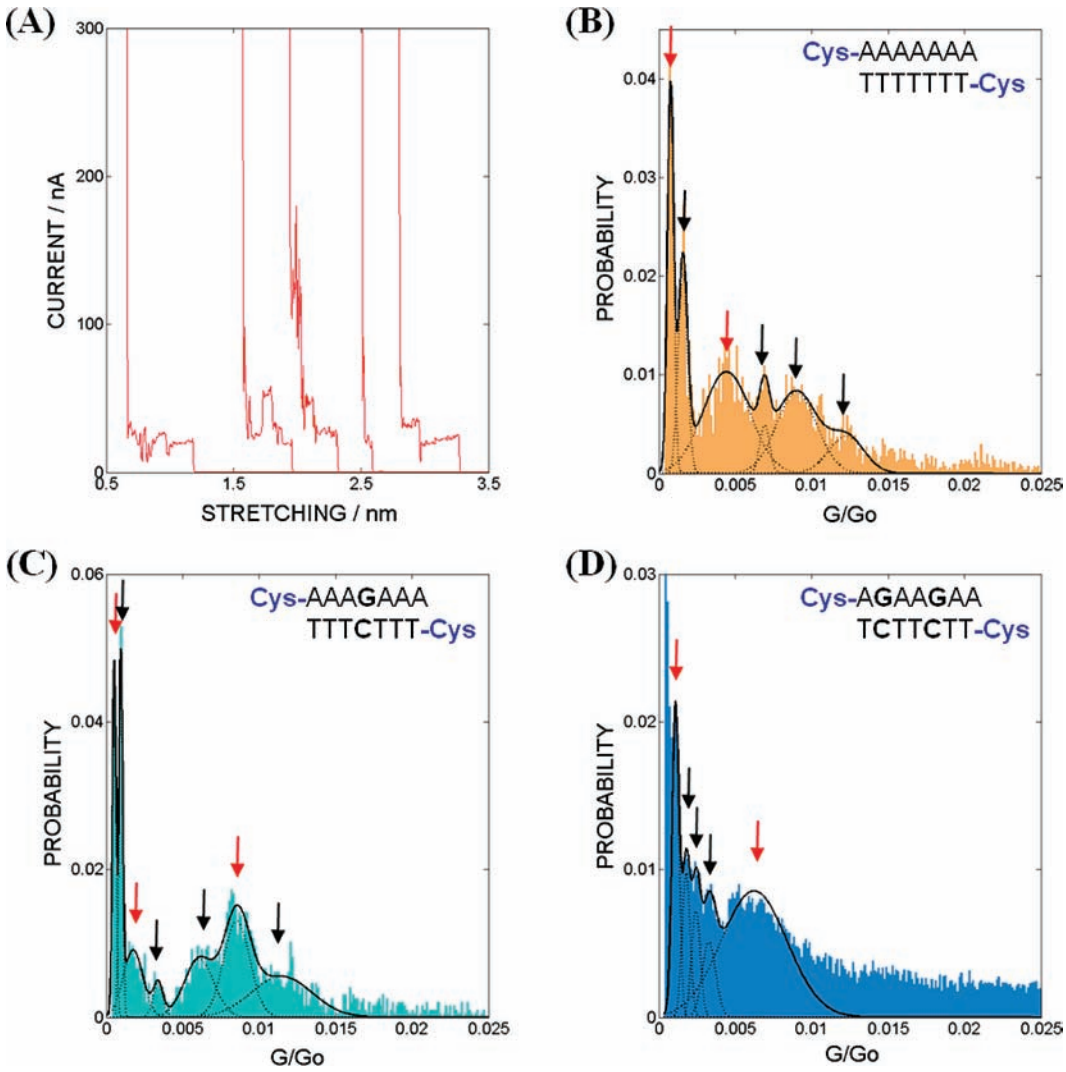

Figure 3. Results of STM-BJ measurements of single-molecule PNA conductance. Panel A shows sample current-distance characteristics recorded for Cys-A_7:Cys-T_7. Panels B, C, and D show the probability distribution of the conductance values measured for the Cys-A_3-A-A_3:Cys-T_3-T-T_3 (B), Cys-A_3-G-A_3:Cys-T_3-C-T_3 (C), and Cys-AAGTTGT:Cys-TTCTTCT (D) molecules trapped within the STM junction. The total number of counts is normalized to 1. Arrows indicate the most commonly observed conductance values. Red arrows indicate fundamental conductance values, which are attributed to the presence of a single molecule in the junction during measurement.

Table 2. Single-Molecule Conductance Values Measured for PNA Duplexes by the STM-BJ Method

	Conductance/$G_0 \times 10^{-3}$				
Probe Strand	Fundamental Values			Mean	Median
Cys-TTT-T-TTT	-	0.76 ± 0.20	4.4 ± 1.5	6.7 ± 5.6	5.5 ± 3.8
Cys-TTT-C-TTT	0.52 ± 0.11	1.8 ± 0.6	8.5 ± 0.8	7.3 ± 5.6	7.4 ± 3.8
Cys-AAGTTGT	-	1.1 ± 0.2	6.2 ± 2.2	8.4 ± 7.1	6.4 ± 4.8

7.4×10^{-3} G_0). The simulation of conductance distributions for each PNA duplex required at least three fundamental conductance values (marked by red arrows in Figure 3B,C), with other peaks corresponding to harmonics or linear combinations of these fundamental values.[26−30] Assuming that each fundamental value represents the conductance of a single molecule, examination of the histograms suggests that no more than four molecules were simultaneously present in the junction during recording of each current-distance curve. The highest value of the fundamental conductance was observed for the PNA containing one GC step. The range of fundamental molecular conductance values does not exceed a factor of 2, which is in agreement with the range observed for the electrochemically determined charge transfer rate constants.

Computational Results. We have calculated σ for the four TA-XY-TA systems assuming two limiting cases for charge transfer: (1) superexchange, where the Fermi level, $E_F = -5.1$ eV is >1.5 eV away from the average HOMO energy of the TA-XY-TA systems (Figure 4C) and (2) near-resonant, where the energy of the Fermi level $E_F = -6.7$ eV is within 0.6 eV of the average HOMO energy for the TA-XY-TA systems (Figure 4D). Note that, in the near-resonant charge transfer limit, thermally induced conformational fluctuations can push the HOMO energies above the Fermi energy for certain PNA conformations (see Figure 7). The computed values of σ are reported in Table S3 of the Supporting Information.

Experimentally, the PNAs with a central GC base pair exhibit larger charge transfer rates than those with a central AT (Figure 3B). In the superexchange limit, the calculated σ for GC-containing PNAs is not always larger than for AT-containing PNAs (Figure 4C). Instead, in the superexchange limit, the calculated σ for duplexes in which all purines were on the same strand (TA-CG-TA/TA-TA-TA) are higher than for duplexes

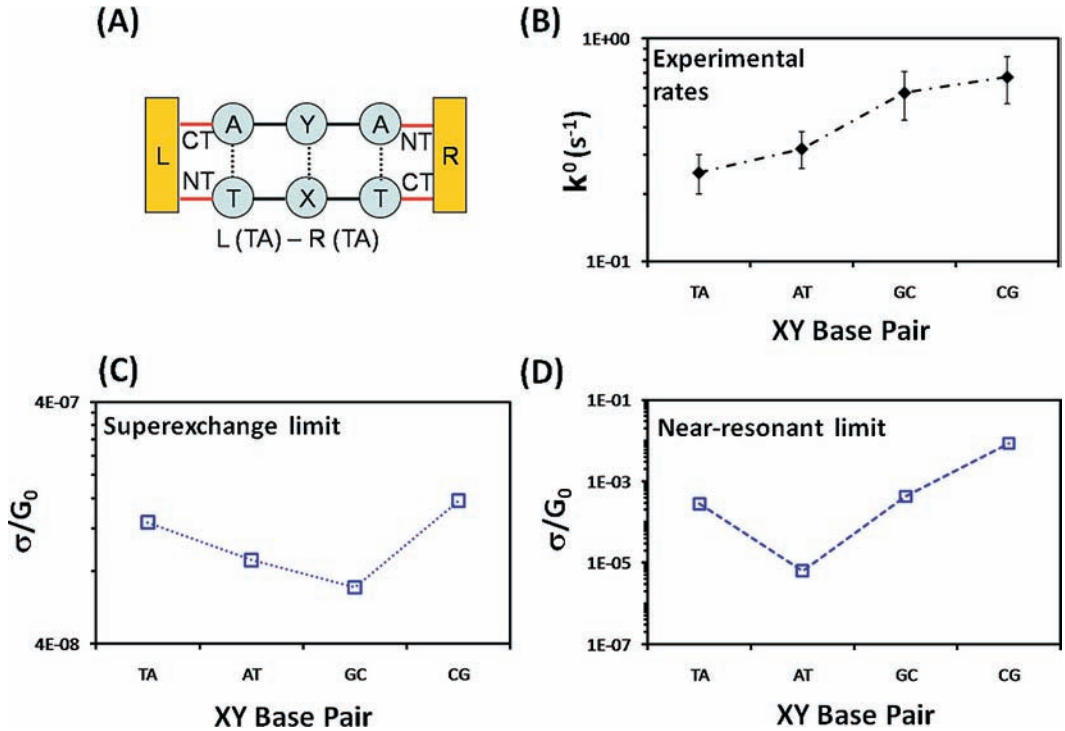

Figure 4. A: Schematic representation of the ds-PNA core unit (AT-XY-AT) used in the conductance calculations, contacted (red lines) to left (L) and right (R) featureless electrodes characterized by a Fermi energy E_F. The labels CT and NT identify the C- and the N-terminus of the PNA fragment, respectively. B: Experimentally observed k^0 values for Cys-$(TA)_3$-(XY)-$(TA)_3$-Fc SAMs on gold electrodes. C and D: Calculated conductance in the superexchange (C) and near-resonant (D) limits of charge transfer as a function of the central nucleobase pair XY for TA-XY-TA PNA fragments. Lines are meant as guides for the eye.

in which the central purine was located on a different strand from the terminal purines (TA-GC-TA/TA-AT-TA). In the near-resonant limit, the calculations reproduce the experimental trend in k^0 and σ, namely that G-containing PNAs have larger k^0 and σ than AT-only PNAs. However, the σ values calculated in both the superexchange and the near-resonant limits are sensitive to the strand placement of the purine, whereas the experimental k^0 and σ values are not.

We hypothesize that the reason for the difference between experimental and theoretical trends is that incoherent scattering processes, which are neglected in the coherent conductance calculations, play a significant role in the charge transfer (*vide infra*). Thus, we performed calculations of the incoherent conductance in the superexchange and near-resonant limits. The model (Figure 5A) explicitly includes pure dephasing on the bridge in terms of a parameter Γ_B, which represents the coupling of bridge electronic states to a Buttiker phase breaker electrode (see Methods). The coupling to the phase-breaking electrode not only includes an additional broadening of the MO energies arising from the bath (solvent plus intramolecular modes not included in the electronic structure calculations) but also introduces a backscattering resistance to conductance, analogous to the back transfer rate in hopping transport created by a localization of the charge on the bridge by the bath. The results presented in Figure 5 show that the calculated near-resonant conductances (Figure 5D) reproduce the insensitivity to the strand placement of the XY purine base. When the bridge dephasing parameter $\Gamma_B = 0$ the (coherent) conductance for TA-CG-TA is much larger than that for TA-GC-TA, however, as we progressively increased the value of Γ_B to 1 eV the conductance for TA-CG-TA drops while the conductance for TA-GC-TA increases to reach the limit σ(TA-CG-TA) $\approx \sigma$(TA-GC-TA). Unlike the TA-CG-TA/TA-GC-TA case, both TA-AT-TA and TA-TA-TA conductances increase with increasing Γ_n values. However, the increase in the conductance of TA-TA-TA as a function of Γ_B is smaller than that for TA-AT-TA so that the conductance trend approaches the limit σ(TA-AT-TA) $\approx \sigma$(TA-TA-TA). Figure 5C shows that the conductances calculated for the superexchange limit with dephasing are unable to reproduce the experimental trends. Hence, we conclude that both dephasing and near-resonant tunneling are needed to rationalize the experimental findings.

We note some caveats of these calculations. The trend in superexchange conductance for $\Gamma_B = 0$ does not match the trend calculated using the full expression for coherent conductance (Figure 4C) because this simplified approach neglects the lower filled molecular orbitals (MOs), which can contribute to the conductance.[11] In our model, we use the same value of bath induced MO energy broadening for all four TA-XY-TA systems and neglect the solvent induced shift of MO energies. This treatment is an oversimplification in light of recent results[31] that show the conductances of poly(AT) DNA sequences might be lowered relative to mixed sequences because of solvent effects. While the results in ref 31 were obtained for DNA in solution (solvent induced broadening and shifts of MO energies are expected to be lower for the PNA packed in a dense monolayer), the trends seen for pure poly (AT) vs mixed (Dickerson dodecamer DNA in ref 31) sequences suggest that including a more rigorous solvent induced shift and broadening of MO energies in our calculations would lower the TA-TA-TA conductance relative to the other three mixed sequences. Such a shift would lead to slightly better agreement of computations (Figure 5D) with experiments (Figure 5B) but would not alter

(31) Woiczikowski, P. B.; Kubar, T.; Gutierrez, R.; Caetano, R. A.; Cuniberti, G.; Elstner, M. *J. Chem. Phys.* **2009**, *130*, 215104.

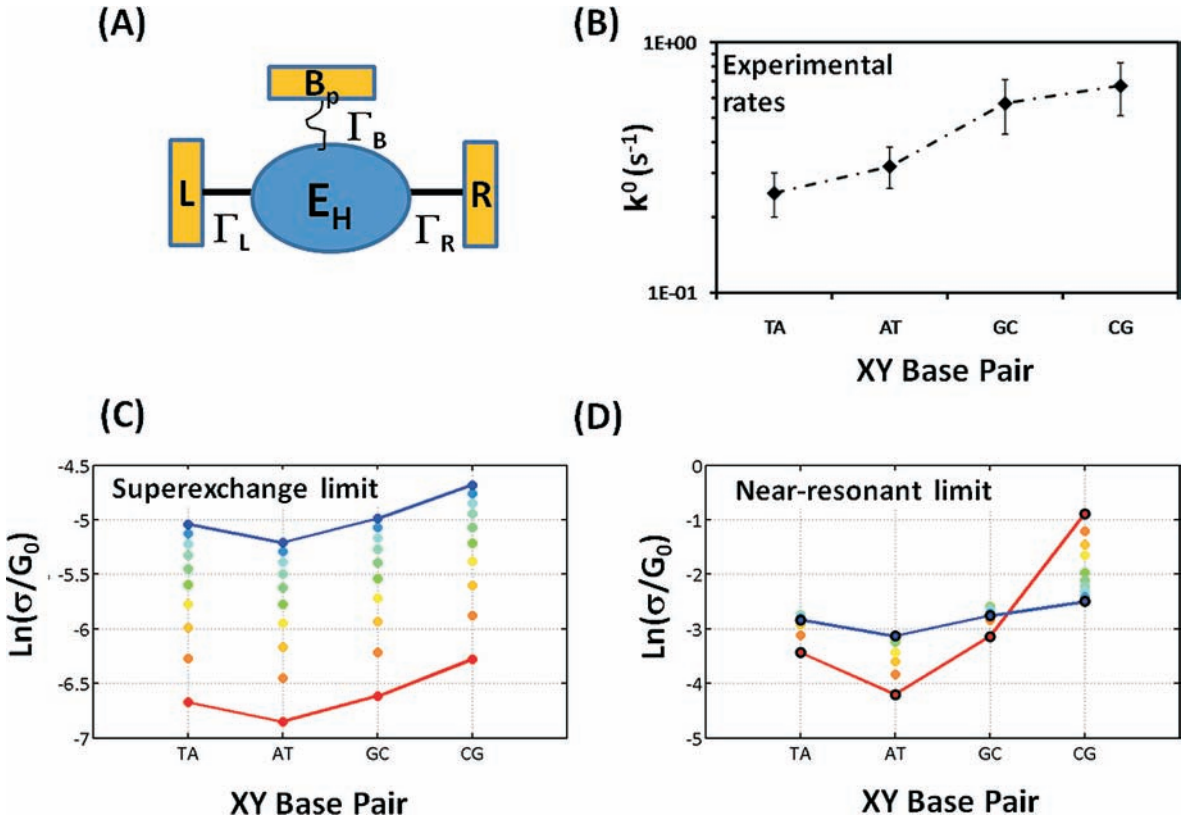

Figure 5. A: Model used to compute the incoherent conductance (see Methods). The bridge is represented by a single energy level E_H coupled to left (L), right (R) and Buttiker phase breaker (B) electrodes. In our calculations $\Gamma_L = \Gamma_R = 0.1$ eV, Γ_B is varied between 0−1 eV and $E_H = \langle E_{HOMO} \rangle$ of the TA-XY-TA systems. B: Experimentally observed k^0 values for Cys-$(TA)_3$-(XY)-$(TA)_3$-Fc SAMs on gold electrodes. C and D: Calculated incoherent conductance in the superexchange (C) and near-resonant (D) limits of charge transfer as a function of the Γ_B (colors red to blue indicate a change in Γ_B from 0 to 1 eV in steps of 0.1 eV) for TA-XY-TA PNA fragments.

the trends and conclusions derived using our simple pure dephasing model. A second point concerns the large coupling value, $\Gamma_B \approx 1$ eV representing pure dephasing. While this value may seem large for a molecular system, we note that it has been introduced in the MO basis and may be interpreted to represent the cumulative effect of dephasing processes acting at different sites along the PNA structure. Previous computational studies of free nucleobases and DNA in solution[32−34] estimated the solvent induced broadening of nucleobase site energies by as much as 0.3−0.4 eV. Despite its simplifying assumptions, the dephasing model used here indicates that the near-resonant conductance with incoherent contributions can reproduce the insensitivity of the charge transfer rate to strand location of the purine in the XY base pair, while the superexchange model cannot capture this effect.

Discussion

Our theoretical simulations are based on a PNA structure obtained by X-ray crystallography.[41] The conclusions drawn based on these calculations are expected to hold for PNA conformations which do not deviate significantly from this geometry. We assume that the dsPNA conformations in the electrochemical rate experiments are close to the crystallographic PNA form because the ellipsometry results show a coincidence between the height of the PNA SAMs and the length of the PNA duplexes estimated based on crystal structure information. This coincidence is not surprising because short nucleic acid duplexes are typically not bent and stand up in the SAM. The good correlation between the electrochemical rates and the oxidation potential of the purine base of the central XY base pair supports the assumption that the PNA duplexes are straight. Since the trends in the STM-BJ conductances closely match the trends in electrochemical rates, this suggests that the geometry of the PNA duplexes in the experimental setup of the conductance measurements is also straight.

We now examine how the near-resonant charge transfer model explains the key experimental observations. The three major observations are as follows: (1) a GC base pair at the XY position leads to about a 2-fold increase in k^0 and σ, relative to an all AT sequence; (2) k^0 is insensitive to the location of the purine base in the XY pair, k^0(CG) = k^0 (GC) and k^0 (AT) = k^0 (TA); and (3) increasing the G content of ds PNA from one to two does not change k^0 or σ. Calculations of the molecular conductance for ds PNA show that the higher k^0 value for PNA duplexes containing G is consistent with near-resonant charge transfer, i.e., a mix of superexchange and resonant mechanisms are manifested.

The Dependence of Charge Transfer on Oxidation Potential. Studies of the solution-phase, photoinduced charge transfer kinetics,[2,3,20,21] and conductivity measurements[35,36] of nucleic

(32) Voityuk, A. A.; Siriwong, K.; Rosch, N. *Angew. Chem., Int. Ed.* **2004**, *43*, 624.
(33) Steinbrecher, T.; Koslowski, T.; Case, D. A. *J. Phys. Chem. B* **2008**, *112*, 16935.
(34) Keinan, S.; Venkatramani, R.; Balaeff, A.; Beratan, D. N. *J. Phys. Chem. C* 2010, ASAP, http://dx.doi.org/10.1021/jp104919g.
(35) Iqbal, S. M.; Balasundaram, G.; Ghosh, S.; Bergstrom, D. E.; Bashir, R. *Appl. Phys. Lett.* **2005**, *86*, 153901.

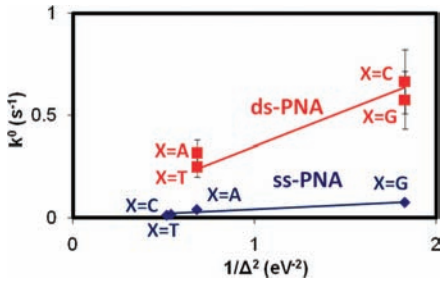

Figure 6. Plot of k^0 with respect to $(1/\Delta_X)^2$ for ss (from ref 11) and ds PNAs (from this study). The lines are guides for the eye.

acids show that the charge transfer efficiency is sensitive to the oxidation potential of the nucleobases. Lewis and co-workers[20] reported an increase in charge separation efficiency and in the rate when one GC pair replaced an AT pair in $(AT)_n$ tracts of $n = 3-6$. Nakatani et al.[21] examined hole transfer between GGG triplets in duplex DNA separated by AAXAA bridges, where X = A, 7-deaza-A, G, or 7-deaza-G. They observed that lowering the ionization potential of X by 0.32 eV (the difference between 7-deaza-A and G) led to a 1.4-fold increase in charge transfer efficiency, as measured by relative strand cleavage at a distal GGG triplet as opposed to the proximal GGG charge injection site. Kawai and co-workers recently demonstrated an increase in charge transfer efficiency and rate upon replacing multiple adenines with diaminopurine[2] or 7-deazaadenine[3] in $(AT)_5$ fragments of a 16 bp duplex. We also found a clear correlation between the oxidation potential of the nucleobase and charge transfer rate for ss PNA, indicating that the charge transfer mechanism is mainly by hole-mediated superexchange.[11]

The relationship we observed between the experimental k^0 and σ for the ds-PNAs (Tables 1 and 2) and the oxidation potential can partially be rationalized by a simplified, McConnell-type, superexchange model.[11] Assuming that the charge transfer is mediated by the purine Pu_{XY}, forming an A_3-$Pu_{XY}A_3$ chain, (Pu_{XY} is the purine of the XY base pair), then the donor−acceptor electronic coupling is:[11]

$$|V| \propto \left(\frac{h_{m-1,m}h_{m,m+1}}{\Delta_m}\right) \quad (1)$$

In eq 1, $h_{m-1,m}$ ($h_{m,m+1}$) is the electronic coupling between the preceding (following) bridge sites with the bridge site $m = Pu_{XY}$, and Δ_m is the energy gap between the Fermi level and the mediating states of the bridge. This energy gap can be approximated using the oxidation potential of Pu_{XY} relative to the oxidation potential of the ferrocene.[11] If we further assume that the couplings $h_{m-1,m}$ and $h_{m,m+1}$ are fixed with variation of Pu_{XY}, then the electronic coupling depends only on the oxidation potential of Pu_{XY}. This simplified superexchange model, henceforth referred to as the modified McConnell superexchange model (MMS), describes the oxidation potential dependence of our ds-PNA data (Figure 6).

Although the MMS model captures the general trend in the data, a more rigorous superexchange calculation (eqs 2 and 3 under Methods) is not consistent with the MMS model (see Figure 4C). When eq 3 (see Methods) is evaluated in the superexchange limit, the tunneling energy E lies far above the HOMO energies of the TA-XY-TA systems. The energy denominator values in eq 3 of the four TA-XY-TA systems are nearly identical. The differences between the calculated σ values for the four TA-XY-TA systems arise from differences in the couplings between the MOs of the bases in the π-stack, i.e., the numerators in eq 3. These couplings are larger for the TA-TA-TA and the TA-CG-TA systems in which the conductance is mediated by direct intrastrand (purines all lie on the same strand) pathways, relative to the TA-AT-TA and the TA-GC-TA systems, in which conductance is mediated by interstrand pathways (purines are distributed on both strands). Thus, the superexchange regime is coupling sensitive, i.e. intrastrand charge-transfer rates are larger than interstrand charge-transfer rates for any central XY base pair.

As shown in Figure 4D, the calculated conductance in a near-resonant model reproduces the experimentally observed dependence of k^0 and σ on the oxidation potential of Pu_{XY}. In this model, the tunneling energy is $E \approx E_{HOMO}$ for the TA-XY-TA systems. Differences in the transmission (and in the rates) among the four TA-XY-TA systems are determined by the first term for m = HOMO in eq 3, which dominates the overall sum because of the small value of the energy denominator. Although differences between interstrand and intrastrand couplings are present in the numerator of the m = HOMO term, the small energy denominators are dominant and determine the trends in the calculated transmission for the four TA-XY-TA systems. Figure 7 and Table 3 show that the HOMO of the TA-CG-TA/TA-GC-TA systems lie closer to the Fermi energy (because of the lower oxidation potential of the G) relative to the HOMO of TA-AT-TA/TA-TA-TA. Thus the near-resonant regime is a more energy sensitive regime and produces the trend σ(TA-CG-TA/TA-GC-TA) > σ(TA-AT-TA/TA-TA-TA), which is consistent with the experimental observations.

Insensitivity of Charge Transfer to Strand Placement of Purines. There have been reports of both a significant kinetic penalty for charge transfer through DNA when an interstrand coupling is required,[22,24] as well as reports indicating otherwise. Kelley and Barton evaluated the efficiency of intrastrand vs interstrand hole transfer in DNA by measuring the fluorescence quenching by guanine or deazoguanine of the nucleobase analogue 1,N^6-ethenoadenine directly incorporated into the base stack.[22] When the hole donor and acceptor were separated by 0−3 bp, they observed higher intrastrand hole-transfer rates. However, as the donor−acceptor separation was increased (from 2−3 bridging bp), the difference between intrastrand and interstrand transfer rates decreased. A kinetic penalty for interstrand crossing was also reported by Long and co-workers in a study of charge transfer through surface-bound 20 bp ds surface-bound ds DNA.[24] They observed a 4-fold decrease in k^0 when the ferrocene and thiol linker were on opposite strands of DNA. In contrast, Kawai and co-workers[3] showed that charge transfer accelerates when one or more (AT) base pairs in a $(AT)_5$ tract within a 16 bp duplex are substituted with nucleobases that have a lower oxidation potential, regardless of the relative strand locations. Their results can be explained if the highest-lying orbitals in both strands contribute to charge transfer through DNA. The experimental results presented in the current study of 7 bp PNA duplexes are not consistent with the observed interstrand penalty for charge transfer through very short (0−3 bp)[22] or long (20-bp)[24] DNA sequences, but they are consistent with the findings of Kawai and co-workers.[3] The similarity in the experimental trends indicates that an intermediate mechanism

(36) Xu, B. Q.; Zhang, P. M.; Li, X. L.; Tao, N. J. *Nano Lett.* **2004**, *4*, 1105.

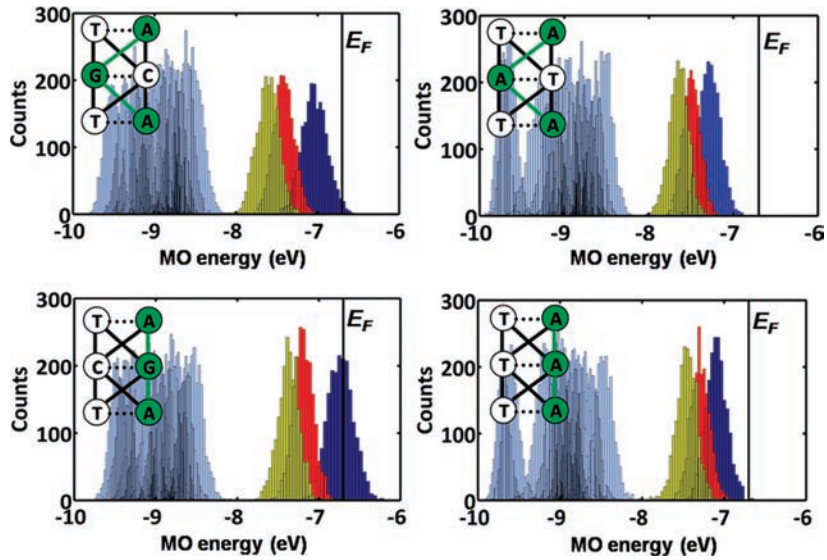

Figure 7. Distribution of filled MO energies obtained for the molecular dynamics-sampled conformational ensemble of the four TA-XY-TA core units. The HOMO, HOMO-1, and HOMO-2 are shown in dark blue, red and yellow, respectively, and are energetically well-separated from the other filled MOs (light blue). The Fermi level in the resonant limit (−6.7 eV) is identified by solid black vertical lines. The inset for each distribution plot is a schematic view of different pathways available for charge transfer. The dominant pathway (green) involves the top three filled MOs, which are mostly localized on the purine bases (green circles; see Supporting Information for details of the extent of localization).

Table 3. Average Energies and Standard Deviations (in eV) for the Highest-Lying Four MOs for the ds PNA Systems

PNA core	energy HOMO (eV)	energy HOMO-1 (eV)	energy HOMO-2 (eV)	energy HOMO-3 (eV)
TA-GC-TA	-7.03 ± 0.15	-7.41 ± 0.13	-7.61 ± 0.13	-8.49 ± 0.10
TA-CG-TA	-6.73 ± 0.16	-7.19 ± 0.12	-7.37 ± 0.13	-8.52 ± 0.10
TA-AT-TA	-7.27 ± 0.12	-7.49 ± 0.10	-7.65 ± 0.11	-8.51 ± 0.09
TA-TA-TA	-7.09 ± 0.13	-7.29 ± 0.11	-7.46 ± 0.12	-8.45 ± 0.11

in the near-resonant regime may operate in both DNA and PNA under some circumstances.

The insensitivity of the experimental k^0 and σ values to the purine placement in the XY base pair is built into the MMS model. The assumption of fixed couplings ($h_{m-1,m}$ and $h_{m,m+1}$) between Pu_{XY} and its nearest neighbor purine bases for the four $(TA)_3$-(XY)-$(TA)_3$ systems, leads directly to equal inter- and intrastrand charge transfer efficiency. On the other hand, our quantitative computational superexchange and near-resonant conductances (Figure 4C,D) are both sensitive to the purine placement in the XY base pair. While the trends in the near-resonant limit are consistent with the observed dependence on oxidation potential (*vide supra*), the computed values of σ(TA-CG-TA) and σ(TA-GC-TA) differ dramatically from each other. How can the insensitivity of the experimental charge transfer rates to the strand interchange of the XY base pair be understood in terms of our more quantitative modeling? The assumption of coherent transport in the computations overestimates the resonant conductance and could lead to large differences between σ(TA-CG-TA) and σ(TA-GC-TA) values. The coupling of the bridge electronic states to a bath (dephasing) is likely to decrease the fraction of resonant transport and to increase the fraction of superexchange transport. Dephasing interactions of the charge on the bridge will introduce a resistance that arises from backscattering and population decay, thereby lowering the resonant transport rate. In contrast, dephasing increases the coherent superexchange transport rate by broadening the electronic levels of the bridge. Analysis of the distributions in Figure 7 shows that more than 40% of the TA-CG-TA PNA conformations are resonant with the Fermi level, i.e., the Fermi level lies within the line width of the HOMO. For the other three systems (TA-GC-TA, TA-AT-TA, and TA-TA-TA) a much smaller fraction (1% or lower) of the conformations exhibit resonant conductance. Because most of the conformations of the TA-CG-TA system exhibit either resonant or near-resonant conductance (Figure 7), we expect dephasing on the bridge to lower its conductance relative to the coherent limit. We also expect bridge dephasing to increase conductances for the TA-GC-TA, TA-AT-TA, and TA-TA-TA systems because most of their conformations are in the superexchange limit (see Fig 5C).

To test the hypothesis formulated above, we calculated the superexchange and resonant conductances, with a description of pure dephasing on the bridge (see Computational Methods). As shown in Figure 5D, including dephasing in the calculation gives TA-CG-TA and TA-GC-TA conductances that are closer than those obtained through the near-resonant calculation in Figure 4D. The difference between the conductances for the TA-AT-TA and TA-TA-TA systems also decreases, thus moving the data more closely in line with the experimental trend. The increase in conductance for the TA-AT-TA system relative to the TA-TA-TA system arises because more of the TA-AT-TA PNA conformations lie in the deep superexchange limit. To summarize, a near-resonant regime with dephasing on the bridge rationalizes the insensitivity of the experimental charge transfer rates to purine placement in the XY base pair.

Guanine Content and Charge Transfer. Several studies have shown that the conductance of surface-bound DNA increases with increasing guanine content.[35−37] Naaman and co-workers[37]

(37) Nogues, C.; Cohen, S. R.; Daube, S.; Apter, N.; Naaman, R. *J. Phys. Chem. B* **2006**, *110*, 8910.

devised a current-sensing AFM technique to measure the conductance of surface-immobilized ds DNA. They found that the resistance of ds 26-bp DNAs containing 0, 8, or 14 GC pairs decreased with the increasing GC content. Iqbal et al.[35] and Xu et al.[36] made similar observations using measurements of DNA conductance in nanogap junctions and STM break junctions, respectively. In contrast, van Zalinge and co-workers[38] observed a much smaller enhancement in charge transfer with increasing guanine content; the conductance of 15-bp ds DNA increased only by a factor of 2 upon moving from 0% to 100% GC content. The results of the electrochemical and STM-BJ measurements for the ds PNAs showed no additional increase in k^0 or σ upon the introduction of a second (GC) base pair into the 7-bp PNA, which agrees with the result obtained for DNA by van Zalinge and co-workers[38] but disagrees with other experiments on DNA.[35−37]

Different charge transfer mechanisms could be at work in our ds PNA systems and in the DNA systems of refs 35−37 (*vide supra*), resulting in different charge transfer rate enhancements upon increasing the G content. Such differences in charge transfer mechanism likely arise from differences in the position of the Fermi level with respect to the molecular orbital energies (the tunneling gap). The tunneling gap in turn depends on the specific experimental configurations that include the sequence studied (all studies in refs 35−38 and our present work use different sequences), the type of nucleic acid (PNA studied here vs DNA studied in refs 35−38), and the molecule−electrode coupling (dependent on terminal capping groups). In the superexchange limit, the energy gap between the DNA/PNA bridge MOs and the Fermi level (donor state) are large. In this case, increasing the G content of the bridge will progressively lower the energy gap, thereby increasing the charge transfer rate as observed in CP-AFM or STM-BJ[35−37] experiments for DNA. However in the near-resonant regime, the energy gap is already very small, so adding a single G to an all-AT, 7-bp DNA/PNA duplex can push the system into resonance (see, for example, Figure 7, left panels). Hence, adding a second G does not increase the efficiency of charge transfer significantly because the system is already resonant prior to the addition of the second G and the PNA length is relatively short. The lack of a k^0 enhancement upon adding a second G cannot be explained in terms of the MMS model and is evidence for a near-resonant charge transfer mechanism, as suggested by the more quantitative modeling.

Superexchange versus Near-Resonant Coupling. The preceding subsections explained how two of the three experimental observations (the correlation of k^0 and σ with the oxidation potential, and their insensitivity to purine placement in the XY base pair) can be explained equally well by the MMS model or by a near-resonance charge-transport model. The MMS model is not consistent with the third experimental result in this work (insensitivity to increasing the G content of the 7bp PNA from one to two) or our previous experimental work,[10] which suggests significant hopping transport contributions for ds PNAs of 7 bp and longer. In this subsection, we use a more detailed computational analysis to show that the basic MMS model assumption, of fixed couplings ($h_{m-1,m}$ and $h_{m,m+1}$) between the Pu_{XY} and its nearest neighbor purine bases, is violated in these 7bp ds PNA systems.

The energy level distributions of filled MOs (Figure 7 and Table 3) suggest that a penalty for interstrand crossing relative to pure intrastrand charge transfer exists in ds PNA. The HOMO, HOMO-1, and HOMO-2 (blue, red, and yellow distributions) are energetically well-separated from the rest of the molecular orbital manifold (light blue distributions) for all four TA-XY-TA PNAs. These three highest-lying filled MOs are primarily localized on the purines (see Supporting Information) and present the dominant channels for charge transfer in these PNA systems. On average, the HOMO, HOMO-1, and HOMO-2 for systems with dominant interstrand pathways (Figure 7, top row and Table 3, first and third rows) are lower in energy than the corresponding orbitals in systems with dominant intrastrand pathways (Figure 7, bottom row, and Table 3, second and fourth row). Taken together with the computed extent of delocalization for each of the three highest-lying filled MOs (Supporting Information, Tables S4−S6 and Figures S2−S4), this observation indicates that a weaker electronic coupling exists between adjacent purine bases located on different strands (interstrand coupling) compared to that between adjacent purines located on the same strand (intrastrand coupling).

We expect the ratio of intra-to-interstrand nucleobase coupling to be larger in PNA than in DNA, because PNA has a smaller base step twist and thus has larger intrastrand base−base overlaps/couplings and smaller interstrand base−base overlaps/couplings than DNA.[39] As such, the sensitivity of charge transfer to the strand location of the purines and/or of the redox acceptor is expected to be higher for PNA than for DNA. On the basis of these considerations, we conclude that the primary premise of the MMS model, namely that the coupling strengths are relatively constant across the four TA-XY-TA systems, does not hold, and that the model does not rationalize the experimental observations.

For the near resonant charge-transfer model, a fraction of the conformations found in ds PNA monolayers should exhibit hopping transport. Our computations indicate that the top three filled MOs, which are well separated from the rest of the MO manifold (see Figure 7), represent the dominant channels for charge transport. Conformational and solvent fluctuations can drive the energies of these three highest-lying orbitals into resonance with the Fermi level. These MOs are localized primarily on the purine A/G bases, which form the "stepping stones" for charge to hop across the PNA bridge. Once on the bridge, the extent of charge (de)localization on the purines is sensitive to the geometry of the bridge[39] and to the solvent environment.[40] A full analysis of the probability of localization on each purine in the sequences is beyond the scope of this study.

Conclusions

The results of these experimental and computational studies demonstrate that the dominant charge transfer mechanism in short PNA duplexes is neither strictly coherent superexchange nor resonant tunneling, but rather, a hybrid of the two mechanisms at the near-resonant limit. The ground state charge transfer rate constant and the conductance of short, 7-bp PNA duplexes are higher for 7-bp PNA containing one GC pair than for 7-bp PNA containing all AT base pairs. The electrochemical measurements show that k^0 is independent of the relative strand location of G, following the trend $(TA)_3$-(GC)-$(TA)_3 \approx (TA)_3$-(CG)-$(TA)_3 > (TA)_3$-(AT)-$(TA)_3 \approx (TA)_3$-(TA)-$(TA)_3$. Increas-

(38) van Zalinge, H.; Schiffrin, D. J.; Bates, A. D.; Haiss, W.; Ulstrup, J.; Nichols, R. J. *ChemPhysChem* **2006**, *7*, 94.

(39) Hatcher, E.; Balaeff, A.; Keinan, S.; Venkatramani, R.; Beratan, D. N. *J. Am. Chem. Soc.* **2008**, *130*, 11752.

(40) Kurnikov, I. V.; Tong, G. S. M.; Madrid, M.; Beratan, D. N. *J. Phys. Chem. B* **2002**, *106*, 7.

ing the G content of an all AT, ds PNA duplex from one to two shows no significant enhancement in the measured charge transfer rate or conductance. The observations of this study for 7-bp PNA, as well as those of Kawai and co-workers,[3] represent a regime of mixed charge-transfer mechanisms. Our theoretical calculations, which consider tunneling as well as resonant charge transport and include bath dephasing effects, show that fluctuations and dephasing modify the bridge energetics so that a mixed charge-transfer mechanism exists. Here, resonant or hopping transport competes with tunneling,[35,36] leading to the observed strand independence of charge transfer in these systems of intermediate length. Our results are consistent with previous experimental work on the distance dependence of charge transfer,[10] which place dsPNA systems of lengths used in the present study at the transition point between pure superexchange and pure hopping charge transport. A general conclusion emerging from our studies is that fluctuations of the duplex structure cause fluctuations of the nucleobase electronic energies and internucleobase couplings in a manner that strongly influences the charge transport mechanism.

Methods

Most aspects of the experimental setup, measurements, and computations were previously reported and discussed.[10−12] A brief description of the methods is provided here. Detailed notes for each method below are given in the Supporting Information.

PNA Synthesis. PNA oligomers with C-terminal cysteine and N-terminal ferrocene moieties were synthesized using previously reported methods, which are described in the Supporting Information.[10−12]

Electrochemical Characterization of PNA SAMs. Gold ball electrodes were prepared and annealed in a manner similar to that described in earlier reports.[10−12] 20 μM ds PNA solutions were prepared in 1:1 v:v acetonitrile/pH 7.0:20 mM sodium phosphate buffer, and annealed in solution by heating at 90 °C for 10 min, followed by slow (∼2 h) cooling to room temperature, in order to ensure duplex formation. The electrodes were then coated with PNA SAMs through immersion in 0.3−1 mL ds PNA solution at 27 °C for 28−40 h. Following incubation, electrodes were washed with deionized water and used directly in electrochemical experiments. Cyclic voltammetry (CV) was performed using a CH Instruments 618B or CHI430 electrochemical analyzer in 1 M $NaClO_4$ (pH ≈ 6−7), with a Ag/AgCl (1 M KCl) reference electrode, a platinum wire counter electrode and a PNA-modified gold wire electrode. Kinetic data were obtained by plotting the peak separation vs scan rate and fitting the data to rate constants based on Marcus theory,[17,18] using a reorganization energy (λ) of 0.8 eV.[17]

Ellipsometric Measurements of PNA Film Thickness. A Gaertner L-117 Null Ellipsometer was used to measure the thickness of the PNA films on gold slides prepared as described previously.[10−12] See Supporting Information for details.

Single Molecule Conductance (STM-Controlled Break Junction) Measurements. All measurements were performed with an Agilent 5500 system equipped with an environmental chamber. The STM head was placed in a homemade, acoustically isolated Faraday cage and placed on an active antivibrational system (Table Stable) located on an optical table. Further technical details of the STM-BJ technique[16] appear in the Supporting Information.

Sample Preparation. ds PNA molecules were hybridized by heating a mixture of complementary strands (20 μM in H_2O: acetonitrile) at 90 °C for ∼10 min, followed by slow (∼2 h) cooling to room temperature. Gold films on mica were modified with PNA via incubation in ds PNA solution for 30 min at room temperature. Samples were rinsed with ethanol and dried under a stream of argon gas prior to experiments.

Conductance Measurements. Experiments were performed using freshly cut gold STM tips (0.25 mm, 99.999% gold wire, Alfa Aesar). Typically, 5−10 tips were used to collect sufficient data for a single PNA sequence. All experiments were performed in bicyclohexyl under an argon atmosphere. A logarithmic preamplifier, calibrated manually with a series of resistors, was used to measure conductance. The measured current was characterized by logarithmic characteristics between 10 nA and 22 μA; currents below 10 nA were not analyzed. Experiments were performed on at least 3 independently prepared samples, resulting in the collection of 20 000−30 000 current-distance characteristics for each type of PNA duplex. A semiautomated filtering procedure (see Supporting Information) was performed to select current-distance characteristics having step-like features; these curves (1−2% of the total data set) were then manually inspected to reject any noisy data. Conductance results were plotted in the form of normalized histograms. Conductance values are expressed in the units of the quantum conductance $G_0 \approx 77\ \mu$S. The histograms were analyzed by fitting Gaussian functions to determine the location of the conductance peaks.

Theoretical Calculations of PNA Structure and Conductance. Since conformational fluctuations can dramatically influence electronic couplings and switch charge-transfer mechanisms in nucleic acids,[42] we performed conductance calculations on an ensemble of dsPNA structures sampled from a molecular dynamics simulation.

Molecular Dynamics Simulations. The initial structures of the four ds PNA sequences, $(TA)_3$-XY-$(TA)_3$ (XY = GC, AT, CG, TA), were constructed with 3DNA[43] based on the average PNA helicoidal parameters from the NMR structure of a PNA octamer[44] (PDB code 2K4G). The structures were solvated, equilibrated and simulated using NAMD[45] with a modified CHARMM force field.[46] During the 2 ns production stage, 2000 snapshots were saved at 1 ps intervals for electronic structure analysis; see Supporting Information for detailed notes.

Electronic Structure Analysis. The electronic structure of the three central base pairs (TA-XY-TA) of the simulated MD structures, referred to in this manuscript as the core unit, was analyzed using single point self-consistent field calculations with the INDO/s method implemented in the CNDO program.[47] The calculated MOs and their energies were used as the input for nonequilibrium Green's function (NEGF) analysis of charge transfer. See Supporting Information for further details.

NEGF Method. The NEGF formalism[48] was previously used to calculate the charge-transfer properties for ss-PNA molecules contacted at the ends by metals.[11] It is assumed that the core unit is connected to the electrodes through the carbon and nitrogen atoms of the flanking T and/or A nucleobase rings (see Figure 4A for the molecule-electrode contact configuration). We assume that the coupling of atoms to the electrodes only broadens the energies of the atomic orbitals and does not affect couplings among atomic orbitals. The coupling between the core unit and the electrode thus represents an effective coupling that includes the effect of the PNA beyond the core unit and the cysteine linkers. The near zero bias conductance is computed using eq 2:[48]

(41) Rasmussen, H.; Kastrup, J. S.; Nielsen, J. N.; Nielsen, J. M.; Nielsen, P. E. *Nat. Struct. Mol. Biol.* **1997**, *4*, 98.
(42) Beratan, D. N.; Skourtis, S. S.; Balabin, I. A.; Balaeff, A.; Keinan, S.; Venkatramani, R.; Xiao, D. *Acc. Chem. Res.* **2009**, *42*, 1669.
(43) Lu, X.-J.; Olson, W. K. *Nucleic Acids Res.* **2003**, *31*, 5108.
(44) He, W.; Hatcher, E.; Balaeff, A.; Beratan, D. N.; Gil, R. R.; Madrid, M.; Achim, C. *J. Am. Chem. Soc.* **2008**, *130*, 13264.
(45) Phillips, J. C.; Braun, R.; Wang, W.; Gumbart, J.; Tajkhorshid, E.; Villa, E.; Chipot, C.; Skeel, R. D.; Kalé, L.; Schulten, K. *J. Comput. Chem.* **2005**, *26*, 1781.
(46) Sen, S.; Nilsson, L. *J. Am. Chem. Soc.* **2001**, *123*, 7414.
(47) Zeng, J.; Hush, N. S.; Reimers, J. R. *J. Am. Chem. Soc.* **1996**, *118*, 2059.
(48) Datta, S. *Quantum Transport: Atom to Transistor*; Cambridge University Press: Cambridge, 2005.

$$\sigma = \frac{q^2}{h} \int T(E)\, F_T(E - E_F)\, dE \qquad (2)$$

where E_F is the Fermi energy. $T(E)$ is the transmission coefficient computed from the INDO/s Hamiltonian as described in ref 11 and in the Supporting Information. The thermal broadening function $F_T\,(E - E_F) = ((1/4k_BT))\cdot\mathrm{sech}^2((E - E_F)/(2k_BT))$ describes the temperature-induced difference between the Fermi functions of the left and right contacts. The zero bias conductance was calculated by assuming two different values for E_F, representative of the superexchange ($E_F = -5.1$ eV) and the resonant ($E_F = -6.7$ eV) transmission limits. The value of E_F in the superexchange limit corresponds to the work-function for Au reported in literature. The value of E_F in the resonant limit is 0.8 eV above the HOMO energy of the G base, in accordance with the oxidation potentials of nucleobases reported by Seidel et al.[19] Two separate models, with and without dephasing, were used to perform conductance calculations.

In the coherent conductance model, which calculates a ballistic current in the resonant limit, the transmission in eq 2 was calculated for each PNA conformation using:[11]

$$T(E) = \sum_m \frac{\Gamma^L_{mm}\Gamma^R_{mm}}{(E - E_m)^2 + \frac{1}{4}(\Gamma^L_{mm} + \Gamma^R_{mm})^2} + \sum_{m\neq n} \frac{\Gamma^L_{nm}\Gamma^R_{mn}}{\left[(E - E_m) - \frac{i}{2}(\Gamma^L_{mm} + \Gamma^R_{mm})\right]\left[(E - E_n) + \frac{i}{2}(\Gamma^L_{nn} + \Gamma^R_{nn})\right]} \qquad (3)$$

The indices m and n run over all MOs. The diagonal elements of the broadening matrix $\Gamma^{L/R}_{mm}$ describe the coupling of orbital m to left or right electrodes.

In the incoherent conductance model, a Buttiker probe electrode (B)[48] is attached to the bridging MOs (Figure 5A) and plays the role of a phase breaker. This calculation assumes that there is no current loss in the electrode B and that there is no mixing of different current channels, i.e., the current at energy E flowing into B from electrodes L/R in Figure 5A is exactly equal in magnitude to the current at energy E flowing out of B to L/R. In this case the effective transmission[48] for charge transfer from electrode L to R is

$$T_{eff} = T_{LR} + \frac{T_{LB} \times T_{RB}}{(T_{LB} + T_{RB})} \qquad (4)$$

where $T_{mn} = \mathrm{Tr}[\Gamma_L G \Gamma_L G^\dagger]$ is the coherent transmission from electrode m to n. The bridge Green's function is given by $G(E) = [EI - H - \Sigma_L - \Sigma_R - \Sigma_B]^{-1}$, where H is the Fock matrix of the molecule and Σ is the self-energy matrix describing molecular eigenstate broadening and shifts induced by coupling to L/R/B electrodes. The broadening matrix is given by $\Gamma_m = i\,[\Sigma_m - \Sigma^\dagger_m]$ for m = L/B/R. The first term in eq 4 is the regular L to R coherent transmission, while the second term is an incoherent transmission for L to R given by a series of two coherent hops: one from L to B and the second from B to L. In our calculations, we assumed that the bridge is represented by a single site energy (the average HOMO energy over the MD structural ensemble) for each TA-XY-TA system (see Figure 5A). The energies of the bridge are assumed to be only broadened and not shifted by their coupling with L/R/B electrodes, i.e., the real parts of the self-energies were neglected in the calculations.

We do not expect the NEGF methods used here to reproduce the absolute values of the experimental conductances for the dsPNA systems. Simplifications concerning the nature of the electrode-molecule coupling, the position of the metal Fermi level relative to the MOs, and the phenomenological model for dephasing (see Supporting Information for a discussion) are substantial. However, the approach is likely robust enough to capture relative charge transport trends between systems that are structurally similar, as shown in the previous studies.[11,49] The relative charge transport trends in the four $(TA)_3$-XY-$(TA)_3$ dsPNA systems used here are captured primarily by the structure of the core TA-XY-TA unit at the center of the strand. The rationale for this core unit choice is that changes in conductance in the four systems are expected to primarily arise from changes in the XY base pair site energies and coupling of the XY pair with the neighboring TA base pairs. Thus, we expect conductance calculations on the core TA-XY-TA fragment, as described here, to capture relative trends in the experimental charge transfer rates and conductance.

Acknowledgment. C.A., D.N.B., and D.H.W. acknowledge support from the U.S National Science Foundation (CHE 0628169). K.L.D. acknowledges support from a Goldblatt Fellowship during part of this research. C.A. acknowledges support by the Sloan Foundation and the Camille and Henry Dreyfus Foundation. D.N.B. acknowledges further support of NSF (CHE-1012357).

Note Added after ASAP Publication. After this paper was published ASAP on December 9, 2010, corrections were made in the second summation in eq 3 and the expression for G(E) in the text following eq 4; the Green's function was also corrected in the Supporting Information. The corrected versions were published December 16, 2010.

Supporting Information Available: Experimental details and characterization for the PNA synthesis, electrochemical measurements, and the electrical conductance measurements. It also includes theoretical and computational details concerning the molecular dynamics simulations, electronic structure calculations, and the conductance calculations. This information is available free of charge via the Internet at http://pubs.acs.org.

JA107622M

(49) Xing, Y. J.; Park, T. H.; Venkatramani, R.; Keinan, S.; Beratan, D. N.; Therien, M. J.; Borguet, E. *J. Am. Chem. Soc.* **2010**, *132*, 7946.